

# PROCEEDINGS OF SPIE

[SPIDigitalLibrary.org/conference-proceedings-of-spie](https://spiedigitallibrary.org/conference-proceedings-of-spie)

## Exploration of alternative mask for 0.33NA EUV single patterning at pitch 28nm

Xu, Dongbo, Gillijns, Werner, Tan, Ling Ee, Philipsen, Vicky, Kim, Ryoung-han

Dongbo Xu, Werner Gillijns, Ling Ee Tan, Vicky Philipsen, Ryoung-han Kim, "Exploration of alternative mask for 0.33NA EUV single patterning at pitch 28nm", Proc. SPIE 11854, International Conference on Extreme Ultraviolet Lithography 2021, 118540T (12 October 2021); doi: 10.1117/12.2599054

**SPIE.**

Event: SPIE Photomask Technology + EUV Lithography, 2021, Online Only

# Exploration of Alternative Mask for 0.33NA EUV Single Patterning at Pitch 28nm

Dongbo Xu, Werner Gillijns, Ling Ee Tan, Vicky Philipsen, Ryoung-han Kim

imec, Kapeldreef 75, B-3001 Leuven, Belgium

## ABSTRACT

Extending 0.33NA EUV single patterning to pitch 28nm will enable metal layers cost-efficiency and significantly shorter process flow for N2 node. At the same time, EUV single patterning becomes very challenging in terms of stochastic defectivity and process window. In this paper, the lithographic performance of the M1 layer of an imec N3 (foundry N2 equivalent) random logic layout is evaluated by means of source mask optimization on these three mask candidates: a standard binary Ta-based absorber mask, a high extinction (high-k) absorber mask and a low-n attenuated phase-shift mask. The impact of mask tonality (bright field vs. dark field) and insertion of sub-resolution assist features on pattern fidelity and process window is evaluated.

**Keywords:** EUV single patterning, SMO, mask absorber, pitch 28nm, logic

## 1. INTRODUCTION

To further reduce the manufacturing cost and process complexity at advanced technology node, the number of layers using extreme ultraviolet lithography (EUVL) patterning will be increased significantly.<sup>1</sup> Therefore, extending 0.33NA EUV single patterning to pitch 28nm is very meaningful to further lower manufacturing cost by replacing multiple patterning, which has been developed and evaluated at imec.<sup>2-5</sup> However, EUV single patterning at pitch 28nm becomes very challenging in terms of stochastic defectivity and process window. The increased importance of stochastic effects at pitch 28nm demands high contrast lithographic images. In EUV lithography, Mask three-Dimensional (M3D) effects have a significant impact on lithographic imaging, which can introduce telecentricity error (TCE), best focus shift and through slit printability issues at wafer level.<sup>6-9</sup> Specifically, the M3D phase differences lead to image contrast loss due to image fading.<sup>4</sup> To mitigate the M3D effects, one approach is to employ alternative masks, high extinction (high-k) absorber masks and low-n attenuated phase-shift masks (PSMs) have been investigated and evaluated in the past.<sup>8,10-18</sup> Another approach is adapting the illumination source shape to mitigate image fading caused image contrast loss due to the M3D effects.<sup>3,4,9,19,20</sup>

In this paper, three mask candidates are studied by using a commercial Source Mask Optimization (SMO) tool, which can help us to find the compromised overall process window of a certain design, and delivers the best source for patterning the given design. The standard binary Ta-based absorber mask is used as the reference. Further more, two alternative mask candidates are included: a high-k absorber mask and a low-n attenuated PSM. In this work, the M1 layer of an imec N3 (foundry N2 equivalent) random logic design is used. To study the patterning performance when using these three mask candidates, various metrics are employed to quantify the patterning quality. Both the impact of mask tonality (bright field vs. dark field) and insertion of sub-resolution assist features (SRAFs) are investigated. To avoid tone inversion and keep low process complexity and cost, dark field EUV mask is employed with positive tone development (PTD) process and bright field EUV mask is combined with negative tone development (NTD) process.

This paper is organized as follows: Section 2 introduces the source mask optimization strategy, and the results of source mask optimization for pitch 28nm Line/Space grating are discussed. Section 3 investigates the patterning performance of the M1 layer of an imec N3 random logic design at pitch 28nm, the impact of mask tonality and insertion of SRAFs on the overall process window (OPW) and patterning quality is evaluated. The last section will provide the summary.

---

Further author information: Dongbo Xu; E-mail: dongbo.xu@imec.be, Telephone: +32 16 28 35 77

## 2. SOURCE MASK OPTIMIZATION STRATEGY

The simulations of the pitch 28nm EUV single patterning case are performed at conditions of ASML 0.33NA NXE:3400 EUV scanner.<sup>21</sup> Three mask candidates are considered, a standard binary Ta-based absorber mask used as the reference, a high-k absorber mask and a low-n attenuated PSM. The binary mask has a 60-nm-thick Ta-based absorber. The absorber thickness of the high-k mask and the low-n attenuated PSM are optimized in the paper, to obtain the best Normalized Image Log-Slope (NILS).<sup>16</sup> The details of multilayer stack information are described in the paper.<sup>22</sup> A blur of 2nm is used in the simulation to mimic the resist blur of assumed patterning process. The SMO-MO (Mask Optimization) flow is used to evaluate the impact of mask tonality and insertion of SRAFs on patterning performance by optimizing model threshold, best focus, and mask correction.

### 2.1 Input Target

Figure 1 shows the design clip that is used for the simulation study in the paper, which is  $1\mu\text{m}^2$  imec N3 random logic design. Analysis of the design helps us to identify yield limiters. As shown in the figure, we deal with various configurations of Line/Space and Tip-to-Tip (T2T) patterns: dense, isolated, semi-isolated with symmetric or asymmetric context. The minimum pitch and minimum trench critical dimension (CD) of 1D features is 28nm and 14nm, respectively. The design retarget is applied on the design to compensate for litho-etch bias from dense to isolated features. Therefore, the trench CD variations are between 14nm for dense features, and up to 18nm for isolated ones. The minimum T2T CD is down to 20nm. The minimum T2T CD is down to 20nm. The red cutlines are used for OPW evaluation in Section 3.1.

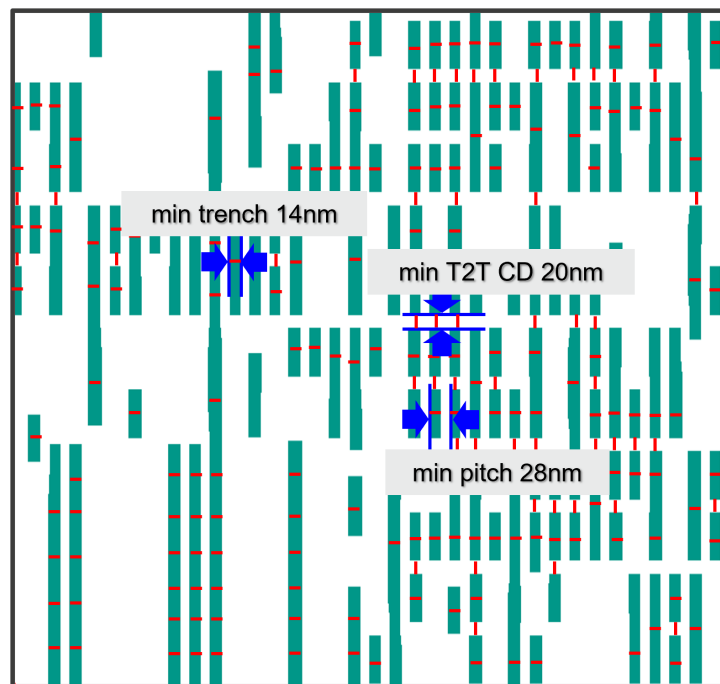


Figure 1: imec N3 random logic design clip with design retarget: minimum pitch is 28nm, the trench CD variations are between 14nm for dense features, and up to 18nm for isolated ones; the minimum T2T CD is 20nm. The red cutlines are used in Section 3.1 for OPW evaluation.

### 2.2 SMO Job Setup

The default EUV SMO template for NXE:3400 in the SMO tool is used. The pupil illumination efficiency is set to 100% and a uniform flare level of 2% is considered.<sup>24</sup> In order to guarantee the required image quality at de-dose, de-focus conditions, four combinations of  $\pm 10\%$  delta dose with  $\pm 40\text{nm}$  delta focus are used in the

optimization. The SMO was first run on a vertical dense pitch 28nm 1:1 Line/Space grating as the input target, this choice is motivated by several aspects:

1. The imec N3 random logic design clip shown in Fig. 1 contains mainly vertical metal trenches, the minimum pitch and minimum trench CD are 28nm and 14nm, respectively;
2. The previous studies have shown that stochastic printing failures are critical in EUVL patterning at tight pitches.<sup>25-27</sup> Higher Image Log-Slope (ILS) is important for EUVL patterning to have good control of the stochastic failures; only using pitch 28nm Line/Space grating as the input target guarantees high ILS on trenches;
3. Patterning various Line/Space is currently our first priority. For now we give a lower priority on T2T;
4. For pitch 28nm Line/Space grating, the area covered by absorber is the same as the open mirror area; therefore, the achieved sources can be used both for bright field and dark field MO evaluation.

### 2.3 Source Optimization for Pitch 28nm Line/Space Grating

Figure 2 shows the optimized sources with respect to these three mask candidates when using vertical pitch 28nm 1:1 Line/Space grating as the input target. All of them are dipole sources with minor difference after source re-rendering. Figure 3 shows the comparison of Exposure Latitude (EL) and NILS for pitch 28nm Line/Space grating with respect to these three mask candidates. The high-k absorber mask and the low-n attenuated PSM are able to increase EL and NILS through focus for pitch 28nm Line/Space grating with respect to the reference binary mask. However, the imec N3 random logic design (Fig. 1) contains not only pitch 28nm Line/Space grating, but also semi-isolated and isolated features, Two-Bars, Three-Bars and short metals at the random patterns region. The achieved SMO sources will be used in Section 3 to evaluate the lithographic performance of this logic design for these three mask candidates.

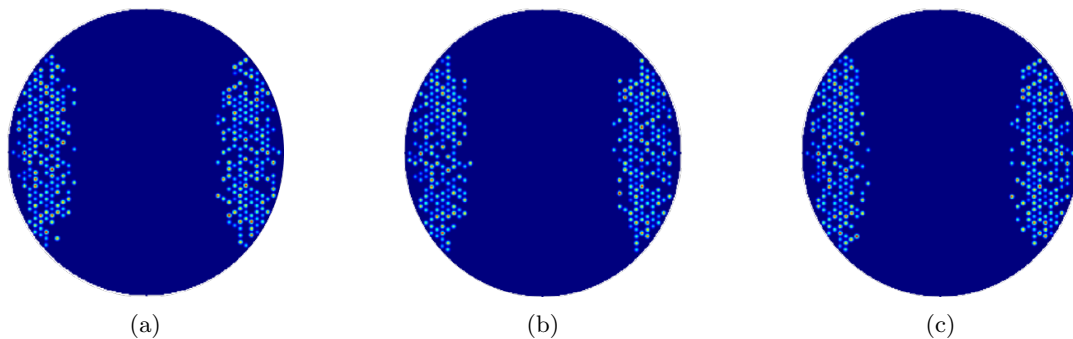


Figure 2: SMO optimized sources with respect to these three mask candidates when using vertical pitch 28nm Line/Space grating as the input target: (a) source for the reference binary mask; (b) source for the high-k absorber mask; (c) source for the low-n attenuated PSM.

## 3. BENEFIT OF ALTERNATIVE MASK CANDIDATES ON PATTERNING PITCH 28NM RANDOM LOGIC DESIGN

This section is focusing on using MO to study and evaluate the impact of these three mask candidates on OPW and patterning quality of EUV single patterning at pitch 28nm, using random logic design as shown in Fig. 1. The used sources are optimized in Section 2.3. In MO jobs, the Mask Rule Check (MRC) constraints are set to 8nm at wafer level scale (1x) for both minimum space and line width, the minimum SRAF CD is set to 6nm (1x). Several metrics are used in our study to evaluate the benefit of these three mask candidates for patterning pitch 28nm vertical design:

1. The CD based OPW is used to characterize the process capability. The Line/Space and T2T CD variations within  $\pm 10\%$  and  $\pm 20\%$  are used in the study to define the process window, respectively; larger OPW indicates better process window tolerance;

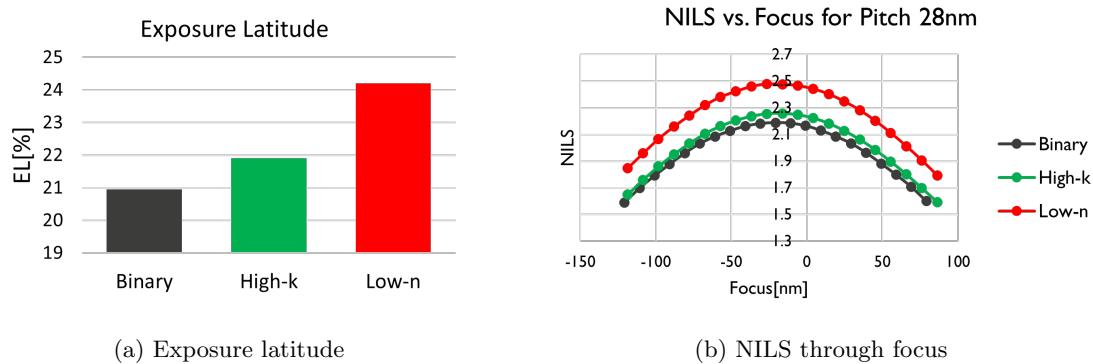


Figure 3: Exposure latitude and NILS through focus for vertical pitch 28nm Line/Space grating with respect to these three mask candidates. The corresponding illumination sources are shown in Fig. 2.

2. The ILS is inversely proportional to stochastic effects. Higher ILS is important for EUVL to have good control of the stochastic variability;
3. The best focus shift of the design features limits the OPW;
4. The Mask Error Enhancement Factor (MEEF) plays an important role in the Design For Manufacturing (DFM) and Resolution Enhancement Technology (RET) flow at advanced technology node. The MEEF of an ideal linear imaging system is one, which means that the wafer CD errors correspond exactly to the mask CD errors.

In the paper, we are focusing on vertical design, and our first priority is for patterning various Line/Space patterns. Since telecentricity error is not pronounced in the center slit and through focus for the vertical Line/Space, it is excluded in our selected evaluation metrics. Our goal is to study the patterning performance when using these three mask candidates, by evaluating the impact of mask tonality and insertion of SRAFs on the selected metrics.

### 3.1 Overall Process Window

#### a) Dark Field Mask

Figure 4 shows the OPWs table of these three mask candidates in dark field with and without insertion of SRAFs. The OPW is calculated on the cutlines appearing in red in Fig. 1. The left column is the OPWs of MO without SRAFs, and the right column is the OPWs of MO with SRAFs. Compared the results of the binary mask MO without SRAFs to MO with SRAFs, the binary mask MO with SRAFs give us the best OPW for patterning pitch 28nm design, which is able to increase both EL and depth of focus (DoF).

Compared the results of the alternative mask candidates to the reference binary mask, the high-k absorber mask increases the EL by ~20% for both MO with and without SRAFs. It is to be mentioned that the low-n attenuated PSM MO without SRAFs does not have OPW due to large best focus shift through pitches. The low-n attenuated PSM MO with SRAFs is able to suppress best focus shift through pitches to obtain a good OPW, which increases the EL by ~10% with respect to the reference binary mask. By insertion of SRAFs, the high-k absorber mask and the low-n attenuated PSM gain more ELs than the reference binary mask. The optimized mask indicates that the high-k absorber mask needs slightly larger SRAFs, while the low-n attenuated PSM requires slightly smaller SRAFs with respect to the reference binary mask. The OPW limiters for each mask candidate are also shown in the Fig. 4:

- The OPWs of the standard binary mask and the high-k absorber mask are limited by best focus shift between isolated and Two-Bar short metals;
- No OPW obtained for the low-n attenuated PSM MO without SRAFs, due to the large best focus shifts among dense Line/Space, Two-Bar, Three-Bar, semi-isolated and isolated features.
- The low-n attenuated PSM with SRAFs insertion reduces best focus shift among different types of features, the limiters are isolated trench between T2Ts and semi-isolated short metals.

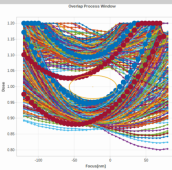
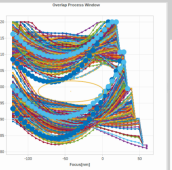
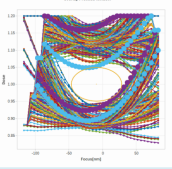
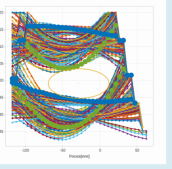
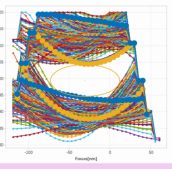
Mask	MO without SRAFs	MO with SRAFs
Binary	 <p>OPW limiters</p> <p>Anchor: 11.6→14nm EL: 9.5% DoF: 94.3nm</p>	 <p>OPW limiters</p> <p>Anchor: 13.87→14nm EL: 10% DoF: 111.36nm</p>
High-k	 <p>OPW limiters</p> <p>Anchor: 11.3→14nm EL: 11.6% DoF: 102.9nm</p>	 <p>OPW limiters</p> <p>Anchor: 14.4→14nm EL: 12.5% DoF: 114.8nm</p>
Low-n	<p><b>No OPW</b></p> <p>OPW limiters:</p> <ul style="list-style-type: none"> <li>• Two-Bar</li> <li>• Three-Bar</li> <li>• Semi-isolated</li> <li>• Isolated</li> </ul>	 <p>OPW limiters</p> <p>Anchor: 13.8→14nm EL: 11.35% DoF: 114.26nm</p>

Figure 4: Overall process windows ( $\pm 10\%$  CD tolerance on trenches,  $\pm 20\%$  CD tolerance on T2Ts) table of dark field masks with and without SRAFs insertion. The OPW is calculated using cutlines shown in Fig. 1. The thick lines on OPW corresponding to the red cutline on the clips in the table, to highlight the OPW limiters.

## b) Bright Field Mask

Figure 5 shows the OPWs table of the reference and alternative mask candidates in bright field with and without insertion of SRAFs. The left column is the OPWs of MO without SRAFs, and the right column is the OPWs of MO with SRAFs. Comparing the results of the binary mask MO without SRAFs and with SRAFs, the binary mask MO with SRAFs is able to enhance the OPW, both for EL and DoF.

Compared to the reference binary mask, for MO without SRAFs case, the high-k absorber mask increases the common depth of focus by  $\sim 10\%$ ; and the low-n attenuated PSM increases the EL by  $\sim 20\%$ . However, the high-k absorber mask and the low-n attenuated PSM MO don't gain anything with SRAFs insertion. The MO output mask layouts indicate that only few SRAFs that are randomly appearing at some locations, which means it is difficult to insert 6nm or larger SRAFs to the mask layout during MO, smaller MRC value is needed for bright field mask. Therefore, the following study in the paper we only consider bright field without SRAFs case. The OPW limiters for each mask type are also shown in the Fig. 5:

- The OPW of the reference binary mask is limited by the best focus shift between Three-Bar and isolated features;
- The OPW of high-k absorber mask is limited by the best focus shift between Three-Bar short metals and more isolated T2Ts;
- The OPW of low-n attenuated PSM is limited by the best focus shift between semi-isolated short metals and isolated features.

In general, the OPW results in Figures 4 and 5 show that for 0.33NA EUV single patterning at pitch 28nm: if the process is limited to a PTD process, a dark field mask with the insertion of SRAFs delivers the best OPW for these three mask candidates; otherwise, a bright field mask without SRAFs using a NTD process delivers the best OPW. Therefore, we will focus on the dark field mask with insertion of SRAFs and the bright field mask without insertion of SRAFs in the following sections for these three mask candidates, to compare in details the relevant imaging metrics.



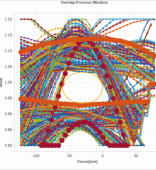
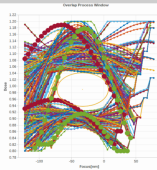
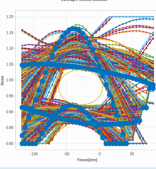
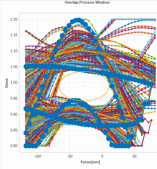
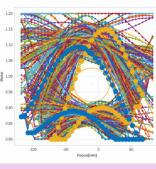
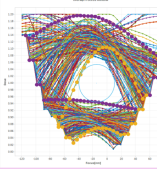
Mask	MO without SRAFs	MO with SRAFs
Binary	 <p>OPW limiters</p> <p>Anchor: 15→14nm EL: 11% DoF: 76.4nm</p>	 <p>OPW limiters</p> <p>Anchor: 12.7→14nm EL: 12.34% DoF: 90.4nm</p>
High-k	 <p>OPW limiters</p> <p>Anchor: 13→14nm EL: 11.5% DoF: 83.34nm</p>	 <p>OPW limiters</p> <p>Anchor: 12.73→14nm EL: 11.2% DoF: 90nm</p>
Low-n	 <p>OPW limiters</p> <p>Anchor: 13.86→14nm EL: 13.5% DoF: 66.96nm</p>	 <p>OPW limiters</p> <p>Anchor: 12.1→14nm EL: 13% DoF: 73.1nm</p>

Figure 5: Overall process windows ( $\pm 10\%$  CD tolerance on trenches,  $\pm 20\%$  CD tolerance on T2Ts) table of bright field masks with and without SRAFs insertion. The OPW is calculated using cutlines shown in Fig. 1. The thick lines on OPW corresponding to the red outline on the clips in the table, to highlight the OPW limiters.

### 3.2 Impact on ILS

#### a) ILS of Trenches at Best Focus

Figure 6 shows the ILS variation map of trenches across the design clip and the corresponding histogram distribution at best focus condition. The ILS map is obtained by densely placing the cutlines on the trenches shown in Fig. 1. The histogram distribution is obtained by binning cutlines per density via design rule check (DRC): the dense bin is the trenches with 28nm pitch to the other trenches on both sides, while semi-isolated bin refers to the trenches with 28nm pitch only on one side and the isolated bin refers to the trenches with more than 28nm pitch on both sides to the other trenches. The top two rows are the ILS map and histogram distribution for dark field MO with SRAFs, and the bottom two rows are the ILS map and histogram distribution of bright field MO without SRAFs:

- The high-k absorber mask in dark field with SRAFs has very similar ILS distribution with respect to the reference binary mask; however, the ILS distribution of the high-k absorber bright field MO without SRAFs is degraded by  $\sim 10\%$ ;
- The low-n attenuated PSM is able to improve the ILS distribution by  $\sim 15\%$  and  $\sim 5\%$  for dark field MO with SRAFs and bright field MO without SRAFs, respectively. More specifically, the low-n attenuated PSM significantly increases the ILS distribution of dense and semi-isolated Line/Space for these two cases; ILS of isolated features gains less improvement.

#### b) ILS of Trenches at $\pm 20\text{nm}$ Defocus

To evaluate the image quality through focus, Fig. 7 shows the ILS histogram distributions on trenches at  $\pm 20\text{nm}$  defocus with respect to the best focus. The top row shows the ILS distributions of dark field MO with SRAFs and bottom row shows the ILS distributions of bright field MO without SRAFs. For dark field MO with SRAFs case, ILS distributions of the high-k absorber mask and the low-n attenuated PSM have a slight ILS degradation of semi-isolated and isolated features at positive defocus with respect to the best focus, while ILS distributions are constant at negative defocus, this behavior is very similar with respect to the reference binary mask; for bright field MO without SRAFs case, ILS distributions of the high-k absorber mask and the binary mask are constant through focus, while the low-n attenuated PSM leads to slight ILS degradation of semi-isolated and isolated features at negative defocus.

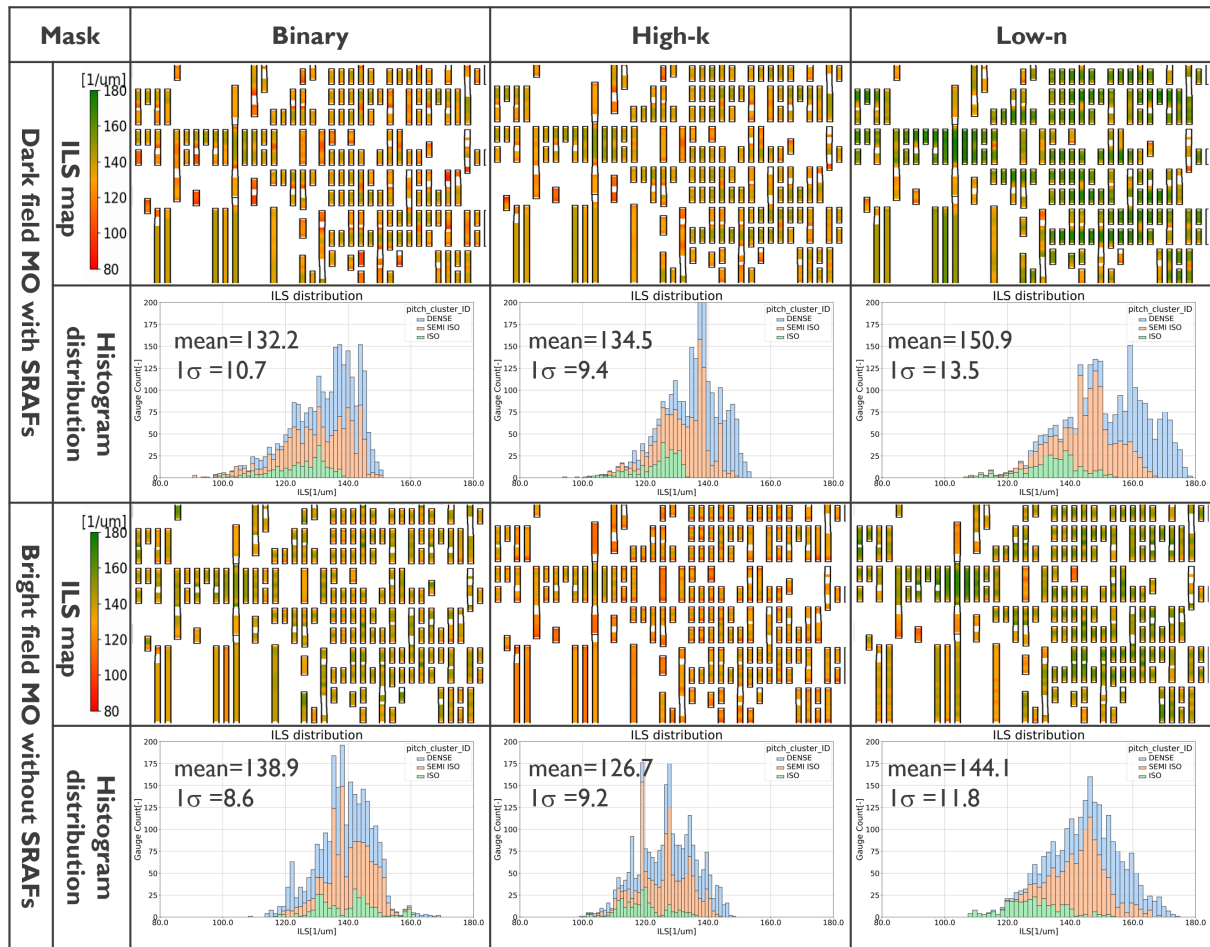


Figure 6: ILS variation map of trenches across the design clip and the corresponding histogram distribution at best focus condition for these three mask candidates.

### c) ILS of T2Ts at Best Focus

Figure 8 shows the ILS histogram distributions on T2Ts at best focus for these three mask candidates. The top row shows the results of dark field MO with SRAFs, and the bottom row is the results of bright field MO without SRAFs. The low-n attenuated PSM provides slightly better ILS for both cases, while the high-k absorber mask delivers slightly worse ILS of T2Ts with respect to the reference binary mask for both cases.

The comparison of ILS distribution among these three mask candidates indicates that, the low-n attenuated is able to provide the best ILS for patterning pitch 28nm vertical design, to have good control of stochastic variability.

## 3.3 Impact on Best Focus Shift

### a) Best Focus Shift of Trenches

Figure 9 shows the best focus shift across the various features on the design clip for these three mask candidates. The high-k absorber mask and the low-n attenuated PSM in dark field MO with SRAFs have smaller best focus shift through pitches with respect to bright field MO without SRAFs case, due to SRAFs have the capability to correct the Bossung tilt and to mitigate the associated best focus shift.<sup>28</sup> For bright field MO without SRAFs case, the best focus shift of the high-k absorber mask is smaller than the reference binary mask, due to high-k absorber in general reduces M3D effects;<sup>8, 11</sup> however, the best focus shift of the low-n attenuated PSM is slightly larger with respect to the reference binary mask, due to more pronounced M3D phase effects.<sup>8, 10, 12</sup>



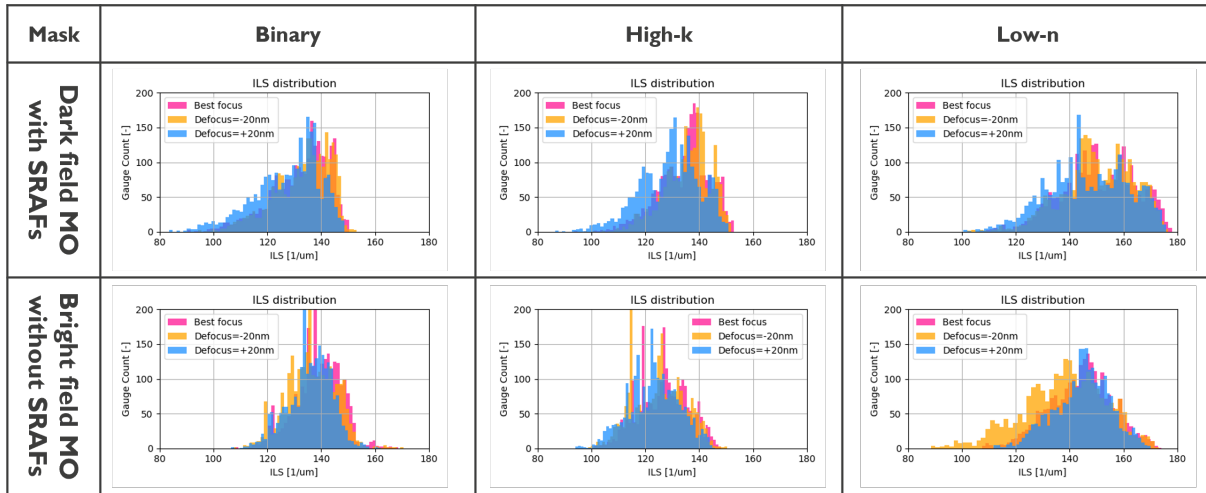


Figure 7: ILS histogram distributions of trenches across the design clip at best focus and  $\pm 20\text{nm}$  defocus for these three mask candidates.

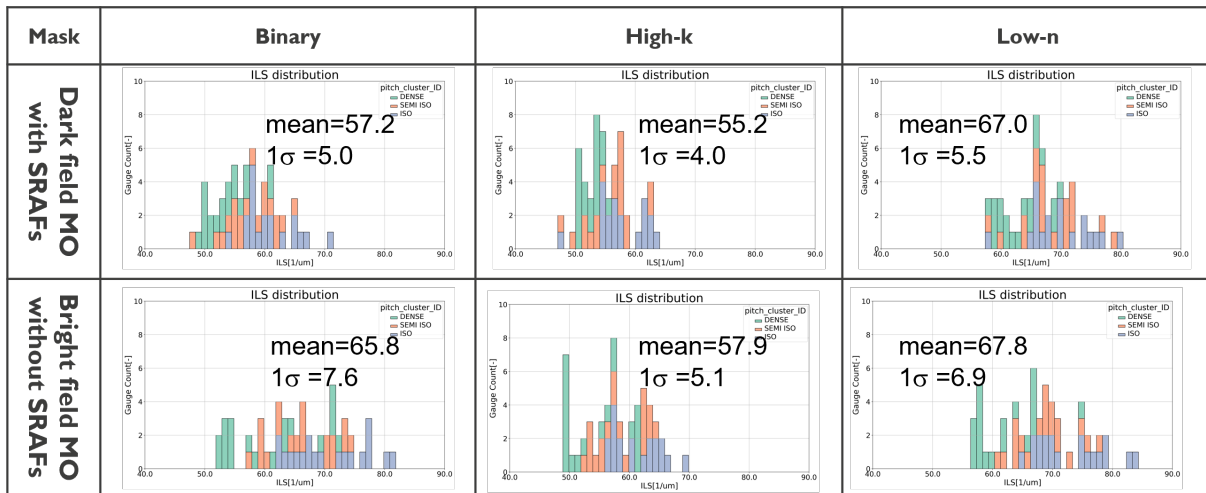


Figure 8: ILS histogram distribution of T2Ts across the design clip at best focus for these three mask candidates.

### b) Best Focus Shift of T2Ts

Figure 10 shows the histogram distribution of best focus shift on T2Ts for both dark field mask with SRAFs and bright field mask without SRAFs for these three mask candidates. The high-k absorber mask and the low-n attenuated PSM have very similar best focus shift of T2Ts with respect to the reference binary mask for both tonality.

Comparing the best focus shift of trenches and T2Ts shown in Fig. 9 and 10 for these three mask candidates, for dark field with SRAFs case, the reference binary mask has largest best focus shift between trenches and T2Ts; and the low-n attenuated PSM delivers the largest best focus shift between trenches and T2Ts for bright field without SRAFs. The high-k absorber mask delivers the smallest best focus shift between trenches and T2T for both tonality.

## 3.4 Impact on MEEF

### a) MEEF of Trenches

Figure 11 shows the MEEF histogram distributions of all the trench features on the design clip. The top row is

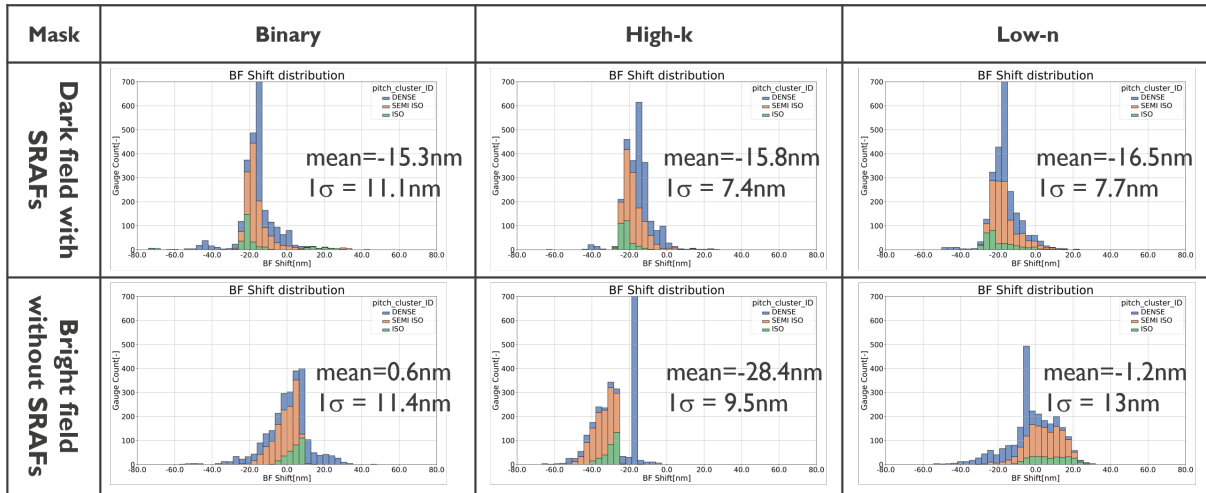


Figure 9: Histogram distribution of best focus shift access all the trenches on the design clip.

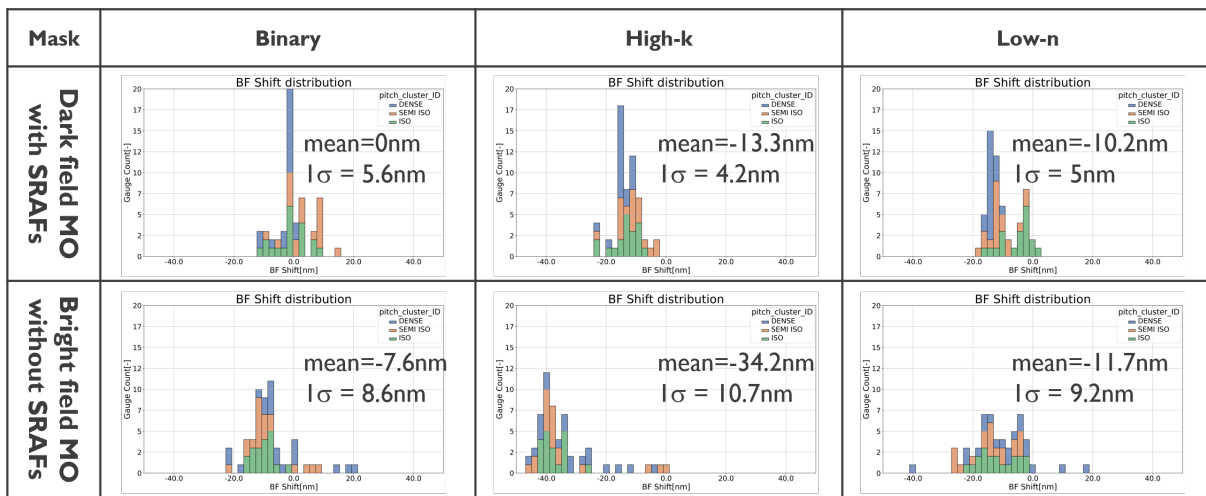


Figure 10: Histogram distribution of best focus shift of T2Ts for all the T2Ts on the design clip.

the MEEF histogram distributions of dark field MO with SRAFs, and the bottom row is the MEEF histogram distributions of bright field MO without SRAFs. The MEEF distribution of the high-k absorber mask is very similar with respect to the reference binary mask for both tonality, while the low-n attenuated PSM improves the MEEF by  $\sim 20\%$  with respect to the reference binary mask for both tonality. It is to be mentioned that the low-n attenuated PSM has a larger MEEF distribution with respect to the reference binary mask and the high-k absorber mask. The low-n attenuated PSM has the MEEF of some isolated features and semi-isolated features is below one, which means that it has the ability to reduce the impact of mask errors rather than amplifying them; and larger mask biasing needed for OPC.

### b) MEEF of T2Ts

Figure 12 shows the MEEF histogram distributions on T2Ts with respect to these three mask candidates for both dark field mask with SRAFs and bright field mask without SRAFs cases. All these three mask candidates have very similar MEEF of T2Ts for each tonality. Comparing the tonality per mask absorber, we can see that MEEF of T2Ts is dominated by mask tonality instead of mask types. The MEEF of T2Ts of bright field without SRAFs is much better than dark field mask with SRAFs. Moreover, simulations also indicate that bright field imaging is able to pattern smaller T2T CD.<sup>4</sup>

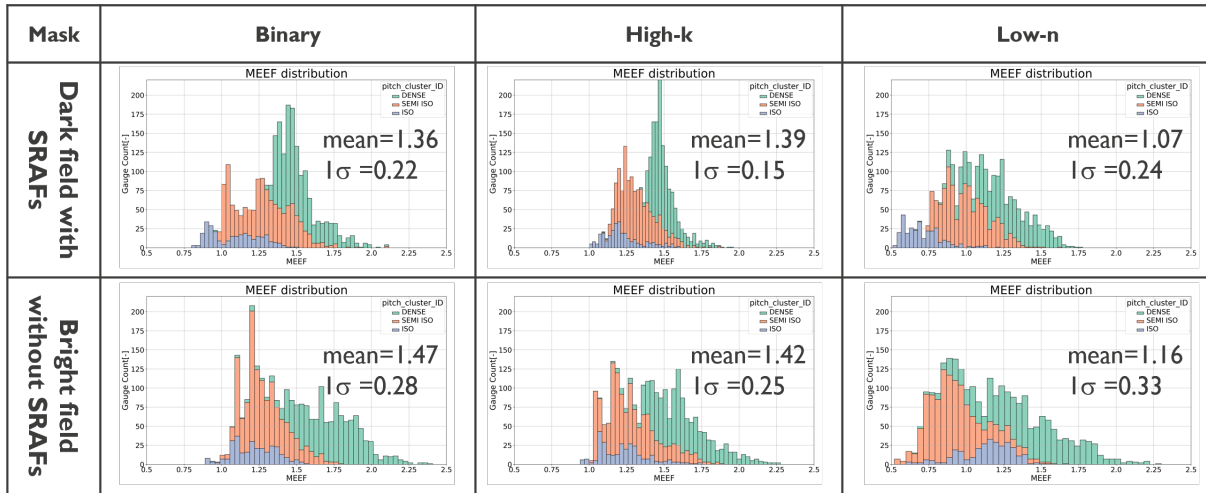


Figure 11: MEEF histogram distribution of all the trench features on the design clip.

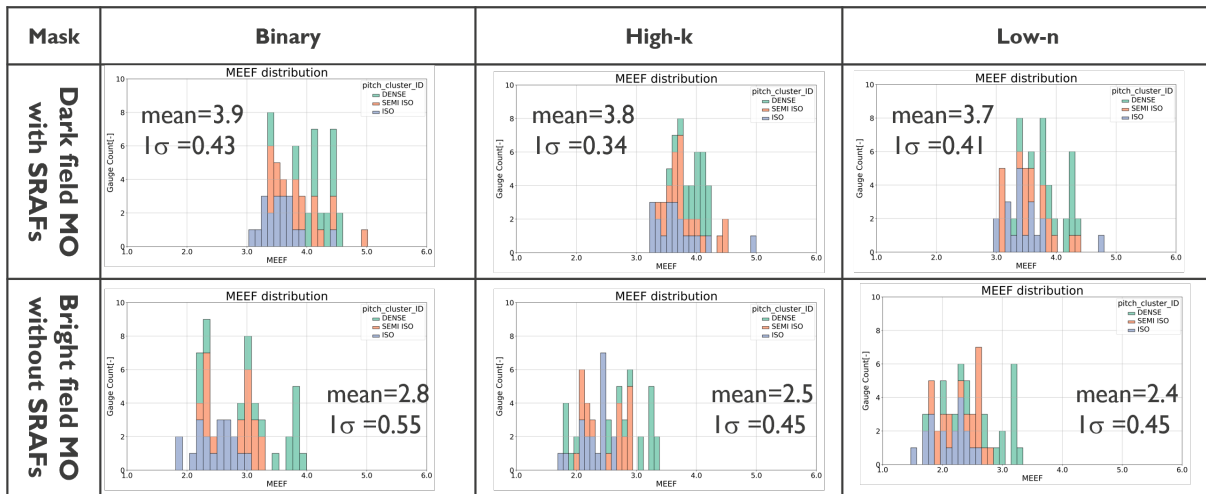


Figure 12: MEEF histogram distribution on T2Ts of all the T2Ts on the design clip.

#### 4. SUMMARY

In this work, three mask candidates for 0.33NA EUV single patterning at pitch 28nm have been explored, using source mask optimization techniques on the M1 layer of an imec N3 random logic design. The impact of both mask tonality and insertion of SRAFs on OPW and pattern fidelity has been studied and evaluated. In general, dark field masks with SRAFs and bright field masks without SRAFs deliver the best OPW. Moreover, the impact of alternative mask candidates on the patterning performance of these two options is quantified over various metrics and compared with the reference binary mask: OPW, ILS, best focus shift and MEEF. The comparative table in Fig.13 summarizes the improvement of each metrics when using these three mask candidates, the best and the worst case for each of the metrics are classified in green and red, respectively.

For dark field mask with SRAFs, the high-k absorber mask enables better EL, smaller best focus shift, with similar ILS and MEEF with respect to the reference binary mask; and the low-n attenuated PSM improves the EL, ILS, best focus shift and MEEF of trenches in average. For bright field mask without SRAFs case, the performance of the high-k absorber mask is very similar with the reference binary mask, expect for slightly worse ILS of trenches, further absorber thickness optimization is required to obtain the best performance; the low-n attenuated PSM improves the EL, ILS and MEEF, but delivers slightly worse DoF. In general, bright field mask

	Mask	OPW		Average ILS[1/um]		Best Focus Shift [average/ $1\sigma$ , nm]		Average MEEF	
		EL[%]	DoF[nm]	Trenches	T2Ts	Trenches	T2Ts	Trenches	T2Ts
Dark field with SRAFs	Binary	<b>10</b>	<b>111</b>	132.2	<b>57.2</b>	<b>-15.3/11.1</b>	<b>0/5.6</b>	1.36	<b>3.8</b>
	High-k	12.5	<b>114</b>	134.5	<b>55.2</b>	<b>-15.8/7.4</b>	<b>-13.3/4.2</b>	1.39	<b>3.8</b>
	Low-n	11.35	<b>114</b>	<b>150.9</b>	<b>67.0</b>	<b>-16.5/7.7</b>	<b>-10.2/5</b>	<b>1.07</b>	<b>3.7</b>
Bright field without SRAFs	Binary	11	76	138.9	65.8	0.6/11.4	-7.6/8.6	<b>1.47</b>	2.8
	High-k	11.5	83	<b>126.7</b>	<b>57.9</b>	-28.4/9.5	<b>-34.2/10.7</b>	1.42	<b>2.5</b>
	Low-n	<b>13.5</b>	<b>67</b>	<b>144.1</b>	<b>67.8</b>	1.2/ <b>13</b>	<b>-11.7/9.2</b>	<b>1.16</b>	<b>2.4</b>

Figure 13: Comparative table summarizes the improvement for each of the metrics when using these three mask candidates for patterning imec N3 random logic design, the best and the worst value for each of the metrics are classified in green and red, respectively.

enables a significant MEEF improvement on T2Ts with respect to the dark field mask. Considering all these aspects, simulations indicate that the low-n attenuated PSM performs the best both for dark field mask with SRAFs and bright field mask without SRAFs for 0.33NA EUV single patterning at pitch 28nm.

Currently, imec is taping out a dark field and a bright field low-n attenuated PSM. Future investigations will focus on mask quality study; and simulations study of low-n attenuated PSM using actual mask stack information and the MRC values measured from the actual mask. Moreover, the optimized source in this paper is only using pitch 28nm Line/Space grating as the input target. Adding T2T clips in the SMO to improve the MEEF of T2Ts for the dark field with SRAFs; and adding semi-isolated feature clips in SMO for the bright field mask without SRAFs, to increase the DoF and reduce the best focus shift will be evaluated. Further more, the TEC through slit for Line/Space and T2T will also be studied for both mask tonality. We will verify the simulation results with wafer data.

## ACKNOWLEDGMENTS

The authors would like to acknowledge all the contributors from ASML at imec: David Rio, Max Delorme.

## REFERENCES

- [1] Ronse, K., Jonckheere, R., Gallagher, E., Philipsen, V., Look, L. V., Hendrickx, E., and Kim, R. H., "EUVL is being inserted in manufacturing in 2019: What are the mask related challenges remaining?," in [35th European Mask and Lithography Conference (EMLC 2019)], Behringer, U. F. and Finders, J., eds., **11177**, 38 – 42, International Society for Optics and Photonics, SPIE (2019).
- [2] Xu, D., Gillijns, W., Drissi, Y., Tan, L. E., Oak, A., and han Kim, R., "EUV single patterning exploration for pitch 28 nm," in [Design-Process-Technology Co-optimization XV], Yuan, C.-M. and Kim, R.-H., eds., **11614**, 125 – 136, International Society for Optics and Photonics, SPIE (2021).
- [3] Rio, D., Adrichem, P. V., Delorme, M., Lyakhova, K., Spence, C., and Franke, J.-H., "Extending 0.33 NA EUVL to 28 nm pitch using alternative mask and controlled aberrations," in [Extreme Ultraviolet (EUV) Lithography XII], Felix, N. M. and Lio, A., eds., **11609**, 63 – 78, International Society for Optics and Photonics, SPIE (2021).
- [4] Franke, J.-H., Frommhold, A., Davydova, N., Aubert, R., Nair, V. V., Kovalevich, T., Rio, D., Bekaert, J., Wang, E., Rispens, G., Maslow, M., and Hendrickx, E., "Metal layer single EUV expose at pitch 28 nm: how bright field and NTD resist advantages align," in [Extreme Ultraviolet (EUV) Lithography XII], Felix, N. M. and Lio, A., eds., **11609**, 43 – 62, International Society for Optics and Photonics, SPIE (2021).

- [5] Simone, D. D., Kljucar, L., Das, P., Blanc, R., Beral, C., Severi, J., Vandenbroeck, N., Foubert, P., Charley, A., Oak, A., Xu, D., Gillijns, W., Mitard, J., Tokei, Z., van der Veen, M., Heylen, N., Teugels, L., Le, Q. T., Schleicher, F., Leray, P., Ronse, K., Kim, I. H., Kim, I., Park, C., Lee, J., Ryu, K., Schepper, P. D., Doise, J., and Kocsis, M., “28nm pitch single exposure patterning readiness by metal oxide resist on 0.33NA EUV lithography,” in [*Extreme Ultraviolet (EUV) Lithography XII*], Felix, N. M. and Lio, A., eds., **11609**, 43 – 53, International Society for Optics and Photonics, SPIE (2021).
- [6] Erdmann, A., Evanschitzky, P., Neumann, J. T., and Graepuner, P., “Mask-induced best-focus shifts in deep ultraviolet and extreme ultraviolet lithography,” *Journal of Micro/Nanolithography, MEMS, and MOEMS* **15**, 1–11 (2016).
- [7] Erdmann, A., Xu, D., Evanschitzky, P., Philipsen, V., Luong, V., and Hendrickx, E., “Characterization and mitigation of 3D mask effects in extreme ultraviolet lithography,” *Adv. Opt. Techn.* **6**, 187–201 (2017).
- [8] Philipsen, V., Luong, K. V., Souriau, L., Hendrickx, E., Erdmann, A., Xu, D., Evanschitzky, P., van de Kruijs, R. W. E., Edrisi, A., Scholze, F., Laubis, C., Irmscher, M., Naasz, S., and Reuter, C., “Reducing EUV mask 3D effects by alternative metal absorbers,” **10143**, 174 – 188 (2017).
- [9] Franke, J.-H., Bekaert, J., Blanco, V., Look, L. V., Wahlisch, F., Lyakhova, K., van Adrichem, P., Maslow, M. J., Schiffelers, G., and Hendrickx, E., “Improving exposure latitudes and aligning best focus through pitch by curing M3D phase effects with controlled aberrations,” in [*International Conference on Extreme Ultraviolet Lithography 2019*], Itani, T., Gargini, P. A., Naulleau, P. P., and Ronse, K. G., eds., **11147**, 50 – 69, International Society for Optics and Photonics, SPIE (2019).
- [10] Burkhardt, M., “Investigation of alternate mask absorbers in EUV lithography,” in [*Extreme Ultraviolet (EUV) Lithography VIII*], Panning, E. M., ed., **10143**, 195 – 208, International Society for Optics and Photonics, SPIE (2017).
- [11] Philipsen, V., Luong, K. V., Opsomer, K., Detavernier, C., Hendrickx, E., Erdmann, A., Evanschitzky, P., van de Kruijs, R. W. E., Heidarnia-Fathabad, Z., Scholze, F., and Laubis, C., “Novel EUV mask absorber evaluation in support of next-generation EUV imaging,” in [*Photomask Technology 2018*], Gallagher, E. E. and Rankin, J. H., eds., **10810**, 53 – 65, International Society for Optics and Photonics, SPIE (2018).
- [12] Erdmann, A., Evanschitzky, P., Mesilhy, H., Philipsen, V., Hendrickx, E., and Bauer, M., “Attenuated PSM for EUV: Can they mitigate 3D mask effects?,” in [*Extreme Ultraviolet (EUV) Lithography IX*], Goldberg, K. A., ed., **10583**, 258 – 270, International Society for Optics and Photonics, SPIE (2018).
- [13] Sejal, R., Philipsen, V., Armeanu, A., Wei, C.-I., Gillijns, W., Lafferty, N., Fenger, G., and Hendrickx, E., “Exploring alternative EUV mask absorber for iN5 self-aligned block and contact layers,” in [*Photomask Technology 2019*], Rankin, J. H. and Preil, M. E., eds., **11148**, 265 – 276, International Society for Optics and Photonics, SPIE (2019).
- [14] van Lare, M.-C., Timmermans, F. J., and Finders, J., “Alternative reticles for low-k1 EUV imaging,” in [*International Conference on Extreme Ultraviolet Lithography 2019*], Itani, T., Gargini, P. A., Naulleau, P. P., and Ronse, K. G., eds., **11147**, 39 – 49, International Society for Optics and Photonics, SPIE (2019).
- [15] Finders, J., de Kruif, R., Timmermans, F., Santaclara, J. G., Connely, B., Bender, M., Schurack, F., Onoue, T., Ikebe, Y., and Farrar, D., “Experimental investigation of a high-k reticle absorber system for EUV lithography,” in [*Extreme Ultraviolet (EUV) Lithography X*], Goldberg, K. A., ed., **10957**, 268 – 276, International Society for Optics and Photonics, SPIE (2019).
- [16] Erdmann, A., Mesilhy, H. S., Evanschitzky, P., Philipsen, V., Timmermans, F. J., and Bauer, M., “Perspectives and tradeoffs of absorber materials for high NA EUV lithography,” *Journal of Micro/Nanolithography, MEMS, and MOEMS* **19**(4), 1 – 16 (2020).
- [17] Wu, M., Thakare, D., de Marneffe, J.-F., Jaenen, P., Souriau, L., Opsomer, K., Soulié, J.-P., Erdmann, A., Mesilhy, H. M. S., Naujok, P., Foltin, M., Soltwisch, V., Saadeh, Q., and Philipsen, V., “Study of novel EUVL mask absorber candidates,” *Journal of Micro/Nanopatterning, Materials, and Metrology* **20**(2), 1 – 13 (2021).
- [18] Philipsen, V., “Mask is key to unlock full EUVL potential,” in [*Extreme Ultraviolet (EUV) Lithography XII*], Felix, N. M. and Lio, A., eds., **11609**, International Society for Optics and Photonics, SPIE (2021).

- [19] Finders, J., van Setten, E., Broman, P., Wang, E., McNamara, J., and van Adrichem, P., “EUV source optimization driven by fundamental diffraction considerations,” in [*International Conference on Extreme Ultraviolet Lithography 2017*], Gargini, P. A., Naulleau, P. P., Ronse, K. G., and Itani, T., eds., **10450**, 55 – 68, International Society for Optics and Photonics, SPIE (2017).
- [20] Armeanu, A., Philipsen, V., Jiang, F., Fenger, G., Lafferty, N., Gillijns, W., Hendrickx, E., and Sturtevant, J., “Enabling enhanced EUV lithographic performance using advanced SMO, OPC, and RET,” in [*International Conference on Extreme Ultraviolet Lithography 2018*], Ronse, K. G., Hendrickx, E., Naulleau, P. P., Gargini, P. A., and Itani, T., eds., **10809**, 85 – 93, International Society for Optics and Photonics, SPIE (2019).
- [21] van de Kerckhof, M., Jasper, H., Levasier, L., Peeters, R., van Es, R., Bosker, J.-W., Zdravkov, A., Lenderink, E., Evangelista, F., Broman, P., Bilski, B., and Last, T., “Enabling sub-10nm node lithography: presenting the NXE:3400B EUV scanner,” in [*Extreme Ultraviolet (EUV) Lithography VIII*], Panning, E. M., ed., **10143**, 34 – 47, International Society for Optics and Photonics, SPIE (2017).
- [22] Makhotkin, I. A., Wu, M., Soltwisch, V., Scholze, F., and Philipsen, V., “Refined extreme ultraviolet mask stack model,” *J. Opt. Soc. Am. A* **38**, 498–503 (Apr 2021).
- [23] Hsu, S., Chen, L., Li, Z., Park, S., Gronlund, K., Liu, H.-Y., Callan, N., Socha, R., and Hansen, S., “An innovative Source-Mask co-Optimization (SMO) method for extending low k1 imaging,” in [*Lithography Asia 2008*], Chen, A. C., Lin, B., and Yen, A., eds., **7140**, 220 – 229, International Society for Optics and Photonics, SPIE (2008).
- [24] Rio, D., Blanco, V., Franke, J.-H., Gillijns, W., Dusa, M., Poortere, E. D., Adrichem, P. V., Lyakhova, K., Spence, C., Hendrickx, E., Biesemans, S., and Nafus, K., “EUV pupil optimization for 32nm pitch logic structures,” in [*International Conference on Extreme Ultraviolet Lithography 2018*], Ronse, K. G., Hendrickx, E., Naulleau, P. P., Gargini, P. A., and Itani, T., eds., **10809**, 104 – 117, International Society for Optics and Photonics, SPIE (2018).
- [25] Levinson, H. J. and Brunner, T. A., “Current challenges and opportunities for EUV lithography,” in [*International Conference on Extreme Ultraviolet Lithography 2018*], Ronse, K. G., Hendrickx, E., Naulleau, P. P., Gargini, P. A., and Itani, T., eds., **10809**, 5 – 11, International Society for Optics and Photonics, SPIE (2018).
- [26] Meli, L., Petrillo, K., Silva, A. D., Arnold, J., Felix, N., Robinson, C., Briggs, B., Matham, S., Mignot, Y., Shearer, J., Hamieh, B., Hontake, K., Huli, L., Lemley, C., Hetzer, D., Liu, E., Akiteru, K., Kawakami, S., Shimoaoki, T., Hashimoto, Y., Ichinomiya, H., Kai, A., Tanaka, K., Jain, A., Choi, H., Saville, B., and Lenox, C., “Defect detection strategies and process partitioning for SE EUV patterning,” in [*Extreme Ultraviolet (EUV) Lithography IX*], Goldberg, K. A., ed., **10583**, 87 – 103, International Society for Optics and Photonics, SPIE (2018).
- [27] Bisschop, P. D. and Hendrickx, E., “Stochastic printing failures in EUV lithography,” in [*Extreme Ultraviolet (EUV) Lithography X*], Goldberg, K. A., ed., **10957**, 37 – 56, International Society for Optics and Photonics, SPIE (2019).
- [28] Mochi, I., Philipsen, V., Gallagher, E., Hendrickx, E., Lyakhova, K., Wittebrood, F., Schiffelers, G., Flier-voet, T., Wang, S., Hsu, S., Plachecki, V., Baron, S., and Laenens, B., “Assist features: placement, impact, and relevance for EUV imaging,” in [*Extreme Ultraviolet (EUV) Lithography VII*], Panning, E. M., ed., **9776**, 513 – 529, International Society for Optics and Photonics, SPIE (2016).